Scattering of periodic solitons

R.J. Cova*
Carleton University, School of Mathematics and Statistics,
1125 Colonel by Drive, Ottawa, Ontario K1S 5B6, Canada,
e-mail: rcova@math.carleton.ca.

W.J. Zakrzewski
University of Durham, Dept of Mathematical Sciences,
Durham DH1 3LE, UK,
e-mail: w.j.zakrzewski@durham.ac.uk

Recibido el 3 de febrero de 2004; aceptado el 21 de abril de 2004

Through numerical simulations we study N-soliton scattering (N=3,4) in the $(2+1)$-dimensional CP^1 model with periodic boundary conditions. Solitons colliding from symmetrical configurations scatter at π/N, as observed in the usual model with standard boundary conditions. When the initial configurations are not symmetric the angles differ from π/N. We describe our observed patterns based on a properly formulated geodesic approximation.

Keywords: Soliton; scattering; CP^1 model.

Usando simulaciones numéricas estudiamos la dispersión de N solitones ($N = 3, 4$) en el modelo CP^1 en (2+1) dimensiones con condiciones de borde periódicas. Las colisiones a partir de configuraciones simétricas dan un ángulo de dispersión π/N, concordando con lo observado en el modelo usual con condiciones de borde estándar. Si inicialmente las configuraciones no son simétricas, los solitones no se dispersan a π/N. Presentamos una descripción de esta dinámica en términos de una aproximación geodésica.

Descriptores: Solitón; dispersión; modelo CP^1.

PACS: 11.10.-z; 02.60.-x; 03.50.Kk

1. Introduction

Physics in $(2+1)$ dimensions is an area of much active research, covering topics that include Heisenberg ferromagnets, the quantum Hall effect, superconductivity, nematic crystals, topological fluids, vortices and solitary waves [1]. Most of these systems are non-linear. In their mathematical description, the well-known family of sigma models plays a starring role. The simplest Lorentz-covariant soliton model in (2+1) dimensions is the CP^1 or non-linear $O(3)$ sigma model. Its solutions, sometimes called 'lumps', are realizations of harmonic maps, a long-established area of research in pure mathematics. However, analytical $O(3)$ soliton solutions have only been found for the static case; the full time-dependent model must be studied using numerical methods and/or other approximation procedures [2].

Sigma models are also useful as low dimensional analogues of field theories in higher dimensions. In effect, the $O(3)$ model in two dimensions exhibits conformal invariance, spontaneous symmetry breaking, asymptotic freedom, and topological solitons, properties similar to those present in a number of important field theories in (3+1) dimensions –like the Skyrme model of nuclear physics [3].

We are concerned with the planar CP^1 model (both in its original and Skyrme-like versions) with periodic boundary conditions where the solitons are harmonic maps $T_2 \mapsto S_2$. A rich diversity of phenomena has been found in this model [4–6], going beyond the two-soliton and annular structures one might expect by analogy with the model with standard boundary conditions, where the soliton fields are harmonic maps $\Re_2 \cup \{\infty\} \approx S_2 \mapsto S_2$.

For planar systems, N identical lumps initially placed at the vertices of a rectangular polygon of N sides, fired with equal speed to collide head-on at the centre of the polygon, scatter and emerge on the vertices of the dual polygon. Such π/N scattering, studied for the CP^1 model on $\Re_2$ in Ref. 7, may be understood on symmetry grounds: the initial data has D_N (dihedral group) symmetry and the time evolution respects that. But imposing periodic boundary conditions breaks the foresaid symmetry, and the interesting question whether dual-polygon scattering still holds for this case must be investigated.

Through numerical simulations on T_2, we confirm the π/N scattering for 3 and 4 identical lumps. The case $N = 2$ has been considered elsewhere [4], and it conforms to the well-documented scattering at 90°. We also look into non-symmetrical configurations (they do not scatter at π/N) and explain the results using the geodesic approximation.

In the following section we introduce our periodic CP^1 model. The numerical procedure is explained in Sec. 3. Sec. 4 analyses collisions between three solitons, and the case $N = 4$ is considered in Sec. 5. In Sec. 6, we present our version of the geodesic approximation which includes the case of initial configurations that are not symmetrical. We find that our predictions (based on this approximation) are in agreement with what is observed in numerical simulations. We close with some concluding remarks in Sec. 7.

2. The CP^1 model on the torus

The non-linear $O(3)$ model involves three real scalar fields $\vec{\phi}(x^\mu) \equiv (\phi_1, \phi_2, \phi_3)$ which satisfy the constraint that $\forall\, x^\mu \equiv (x^0, x^1, x^2) = (t, x, y) \in T_2$ the fields lie on the unit sphere S_2:

$$\vec{\phi}.\vec{\phi} = 1. \tag{1}$$

Subject to this constraint, the Lagrangian density of the system is

$$\mathcal{L} = \tfrac{1}{4}\left(\partial_\mu \vec{\phi}\right).\left(\partial^\mu \vec{\phi}\right). \tag{2}$$

The invariance of this Lagrangian under global $O(3)$ rotations in field-space is apparent.

The model is conveniently recast in terms of one independent complex field W (the CP^1 formulation) related to $\vec{\phi}$ via

$$\vec{\phi} = \left(\underbrace{\frac{W+\bar{W}}{|W|^2+1}}_{\phi_1}, \underbrace{i\frac{-W+\bar{W}}{|W|^2+1}}_{\phi_2}, \underbrace{\frac{|W|^2-1}{|W|^2+1}}_{\phi_3} \right). \tag{3}$$

The Lagrangian (2) now reads

$$\mathcal{L} = \frac{|\partial_t W|^2 - 2|\partial_z W|^2 - 2|\partial_{\bar{z}} W|^2}{(1+|W|^2)^2}, \tag{4}$$

where $z = x + iy$ and $\bar{z} = x - iy$. For all t, the fields W are mappings from the torus T_2 to the sphere S_2, *i.e.*, they satisfy the periodic boundary conditions

$$W(z + mL + inL) = W(z), \tag{5}$$

where $m, n = 0, 1, 2, \ldots$ and the period L denotes the size of the square torus.

The *static* soliton solutions of the model are thus doubly periodic functions of z, that is, elliptic functions that may be expressed through the Weierstrass σ-function as [8, 9]:

$$W = \lambda \prod_{j=1}^{\kappa} \frac{\sigma(z-a_j)}{\sigma(z-b_j)}, \qquad \sum_{j=1}^{\kappa} a_j = \sum_{j=1}^{\kappa} b_j. \tag{6}$$

The complex number λ is related to the overall size of the solitons, the zeros a_j and poles b_j determine their sizes and positions on T_2, and the positive integer κ is the order of the elliptic function W.

The static energy density (or potential energy density) associated with (6) can be read-off from (4):

$$E = 2\frac{|\partial_z W|^2 + |\partial_{\bar{z}} W|^2}{(1+|W|^2)^2}. \tag{7}$$

Pictures of this energy distribution reveal the familiar CP^1 lumps, as those of Fig. 1 for example.

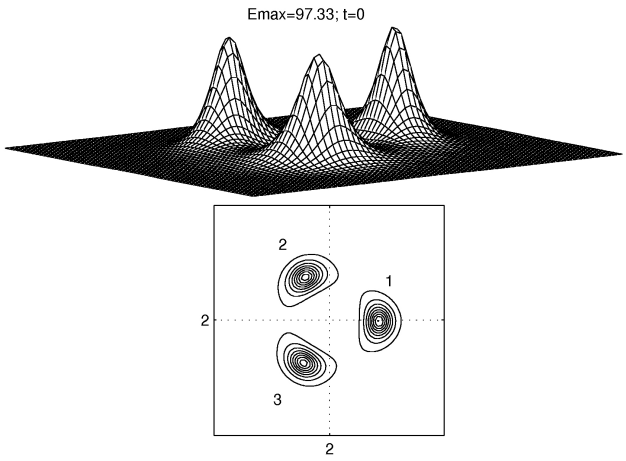

FIGURE 1. The energy distribution for N=3 at the initial time, both in three dimensional and contour plot forms.

The energy is related to the topological charge by the Bogomolnyi bound

$$E \geq 2\pi|N|. \tag{8}$$

The instanton solutions correspond to the equality in (8): solutions carrying $N > 0$ ($N < 0$) imply $\partial_{\bar{z}} W = 0$ ($\partial_z W = 0$), the Cauchy-Riemann conditions for W being an analytic function of z ($\bar{z}$). Note that the simplest non-trivial elliptic function is of the order of two, hence there are no single-soliton solutions on T_2.

We utilize the pure model (4) for $N = 3$, but for $N = 4$ the energy involved is so large that the well-known instability of the planar model (recall that its conformal invariance means that the lumps can have any width) breaks the numerical procedure fast. A stabilising Skyrme term must be introduced for this case.

3. Numerical procedure

In this paper we want to discuss time dependent solutions of the model (4) and its Skyrme version [see equation (24)], where the time dependence describes the movement of solitons. As we do not have analytical time-dependent solutions, we resort to numerical simulations. For this we take fields of the form (6) as the initial conditions. Since during the simulations the field W may become arbitrarily large, we have preferred to run our simulations in the ϕ-formulation of the model.

Strictly speaking, truly independent solitons can only be obtained in the asymptotic regime of large soliton separation, which really never happens on a compact manifold such as T_2. However, each factor $W_j \equiv \sigma(z-a_j)/\sigma(z-b_j)$ in (6) (when $a_j \sim b_j$) roughly represents one soliton, providing a setting to study more or less independent structures. The present work is limited to systems in the topological classes 3 and 4. These systems move, collide and scatter off upon being set into motion by boosting each W_j separately. The initial-value problem is then completely specified by giving both $W(t)$ and $\partial_t W(t)$ at the initial time $t = 0$.

For a square torus we have the so-called lemniscatic case [10] where σ possesses the simple Laurent expansion

$$\sigma(u) = \sum_{j=0}^{\infty} G_j u^{4j+1}, \qquad G_j \equiv G_j(L) \in \Re. \tag{9}$$

For the accuracy of our calculations it is sufficient to compute the series (9) up to G_5 (our coefficients for $j > 5$ are negligible):

$$\left.\begin{array}{rcl} G_0 &=& 1 \\ G_1 &=& -0.7878030 \\ G_2 &=& -0.221654845 \\ G_3 &=& 9.36193 \times 10^{-3} \\ G_4 &=& 7.20830 \times 10^{-5} \\ G_5 &=& 2.37710 \times 10^{-5} \end{array}\right\}.$$

We have employed the fourth-order Runge-Kutta method, and approximated the spatial derivatives by finite differences. The Laplacian has been evaluated using the standard nine-point formula, and to further check our results a 13-point recipe has also been used. Respectively, the Laplacians are:

$$\nabla^2 = \frac{\begin{bmatrix} 1 & 4 & 1 \\ 4 & -20 & 4 \\ 1 & 4 & 1 \end{bmatrix}}{6 \times (\delta x)^2},$$

$$\nabla^2 = \frac{\begin{bmatrix} & & -1 & & \\ & 1 & 12 & 1 & \\ -1 & 12 & -48 & 12 & -1 \\ & 1 & 12 & 1 & \\ & & -1 & & \end{bmatrix}}{10 \times (\delta x)^2}. \tag{10}$$

The discrete model has been evolved on a $n_x \times n_y$=200×200 square periodic lattice with spatial and time steps δx=δy=0.02 and δt=0.005, respectively. The vertices of the fundamental period cell we have used for our simulations were at

$$(0,0),\ (0,L),\ (L,L),\ (L,0), \quad L = n_x \times \delta x = 4. \tag{11}$$

Unavoidable round-off errors have gradually shifted the fields away from the constraint $\vec{\phi}.\vec{\phi} = 1$. So, like in the planar case [11], to correct this we have rescaled $\vec{\phi} \to \vec{\phi}/\sqrt{\vec{\phi}.\vec{\phi}}$ every few iterations. Each time, just before the rescaling operation, we have evaluated the quantity $\mu \equiv \vec{\phi}.\vec{\phi} - 1$ at each lattice point. Treating the maximum of the absolute value of μ as a measure of the numerical errors, we have found that $\max|\mu| \approx 10^{-8}$. This magnitude is useful as a guide to determine how reliable a given numerical outcome is. Usage of unsound numerics in the Runge-Kutta evolution shows itself as a rapid growth of $\max|\mu|$; this also occurs, for instance, when the solitons pinch-off.

The parameter λ in (6) has been set to $\lambda = (1,0)$ all throughout.

4. Three solitons

First we have considered states with three solitons. Our initial configuration is given by taking $\kappa = 3$ in (6), the elliptic function of order 3

$$W = \frac{\sigma(z-a_1)}{\sigma(z-b_1)} \frac{\sigma(z-a_2)}{\sigma(z-b_2)} \frac{\sigma(z-a_3)}{\sigma(z-b_3)},$$

$$\sum_{j=1}^{3} a_j = \sum_{j=1}^{3} b_j. \tag{12}$$

The values of a_j, b_j have been selected in such a way that the solitons lie symmetrically around a circle in the network (11). This is easily achieved by fixing a_1, b_1 to reasonable values and setting

$$\left.\begin{array}{rcl} a_1' &=& a_1 - c \\ b_1' &=& b_1 - c \end{array}\right\}, \tag{13}$$

where $c = (2,2)$ stands for the centre of the period cell. Then

$$\left.\begin{array}{l} a_j'{=}a_1' \exp(i\beta_j) \\ b_j'{=}b_1' \exp(i\beta_j) \end{array}\right\}; \quad \beta_j{=}(j-1)\frac{2\pi}{3},\ j{=}1,2,3. \tag{14}$$

This symmetrical arrangement gives solitons of the same size, and satisfies the selection rule in (12) for any choice of the complex numbers a_1', b_1':

$$\sum_{\kappa=1}^{3} a_j' = (0,0) = \sum_{\kappa=1}^{3} b_j'. \tag{15}$$

Next we go back to a_j and b_j through

$$\begin{aligned} a_j &= a_j' + c \\ b_j &= b_j' + c \end{aligned} \tag{16}$$

and supply the system with an initial speed v_0 by boosting

$$\left.\begin{array}{rcl} a_j &\to& a_j + v_j t \\ b_j &\to& b_j + v_j t \end{array}\right\}; \quad v_j = -v_0 \exp(i\beta_j). \tag{17}$$

It is now possible to evaluate the time derivative of W at the initial time. Inserting (17) into (12) we get

$$\begin{aligned} \partial_t W(t) \mid_{t=0} = [&(\partial_t W_1) W_2 W_3 + W_1 (\partial_t W_2) W_3 \\ &+ W_1 W_2 (\partial_t W_3)]_{t=0}, \end{aligned} \tag{18}$$

where

$$\partial_t W_j(t) \mid_{t=0} = -v_j \left[\frac{\partial_z \sigma(z-a_j)}{\sigma(z-a_j)} - \frac{\partial_z \sigma(z-b_j)}{\sigma(z-b_j)}\right] W_j,$$

$$W_j \equiv \frac{\sigma(z-a_j)}{\sigma(z-b_j)}. \tag{19}$$

Our initial-value problem is defined by (12) and (18)-(19). Choosing

$$\left.\begin{array}{l} a_1 = (3,2) \\ b_1 = (1.45, 1.95) \\ v_0 = 0.35 \end{array}\right\}, \tag{20}$$

gives an initial configuration whose energy density is exhibited in Fig. 1. The solitons are placed on the vertices of an equilateral triangle; the first lump is situated along the line y=2 at $\beta_1 = 0°$, with respect to which solitons 2 and 3 are rotated $\beta_2 = 120°$ and $\beta_3 = 240°$, respectively. These angles are readily checked from the picture with the help of a protractor.

The results of simulations for this case are depicted in Fig. 2 for various times. The three solitons are fired towards the centre of the triangle, and in so doing they expand (the peak E_{max} of the energy density decreases). The solitonic trio collides head-on and coalesces in a ringish structure, then emerging towards the vertices of the dual triangle, that is, the initial line of approach of a given incoming soliton forms an angle of $\pi/3$ with the line along which an outgoing, emerging soliton progresses. This $\pi/3$ scattering can be best appreciated in Fig. 3, where both the initial state (t=0) and the final state ($t = 2$) are displayed together.

Returning to Fig. 2 we see that E_{max} becomes narrower with time, particularly after the lumps scatter off and start drawing away from each other. At $t = 2$, for instance, the maximum value of the energy density goes up to $E_{max} = 579.37$. Soon after $t > 2$, this peak gets so spiky that the numerics breaks down: the instability of the planar $O(3)$ model takes over and leads to singularity formation.

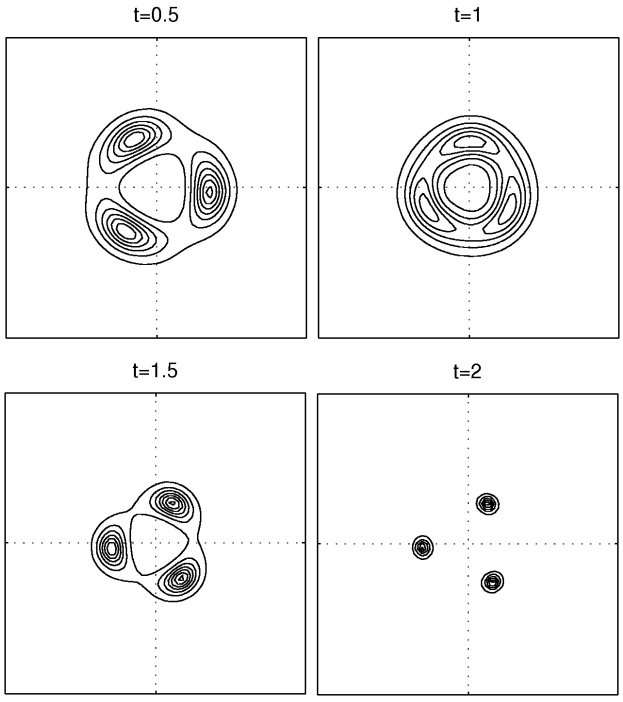

FIGURE 2. The evolution of the three lumps of Fig. 1 at various times.

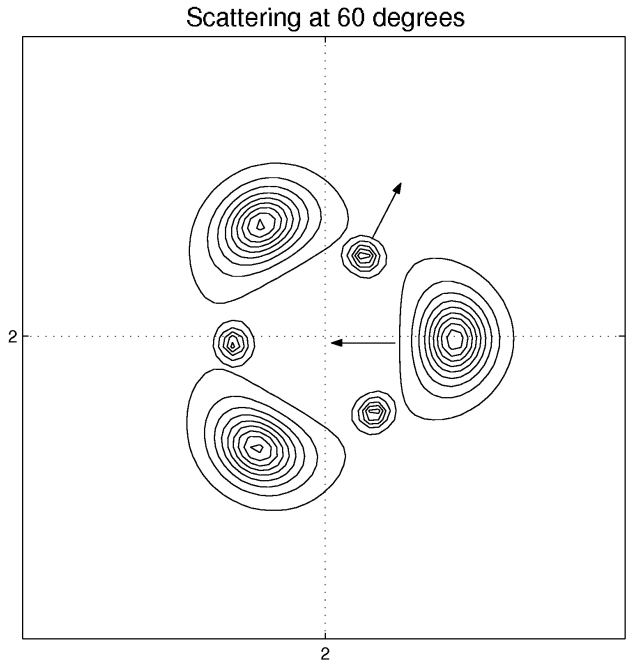

FIGURE 3. Scattering at $\pi/3$ radians.

Our result is noteworthy: the initial configuration, although positioned at the vertices of an equilateral triangle in the period cell, does not produce D_3 symmetry because the torus itself, being homogeneous but not isotropic, has no such symmetry (the fundamental grid has directed sides). One could reasonably expect the lumps to scatter along directions that need not respect D_3 symmetry. Therefore, the rationale applied to explain π/N scattering for the model on $\Re_2$ is no longer valid for the model with periodic boundary conditions.

However, we observe that as the solitons are well localized the boundary conditions may not be very important, and our numerical results are consistent with this expectation. To test this further, we could place the solitons nearer the edges of the grid and see whether we still observe $60°$ scattering. We hope to investigate this issue in the future.

5. Four solitons

Next we have looked at the $N = 4$ configurations. The initial field is given by the elliptic function of order 4

$$W = \frac{\sigma(z-a_1)}{\sigma(z-b_1)}\frac{\sigma(z-a_2)}{\sigma(z-b_2)}\frac{\sigma(z-a_3)}{\sigma(z-b_3)}\frac{\sigma(z-a_4)}{\sigma(z-b_4)},$$

$$\sum_{j=1}^{4} a_j = \sum_{j=1}^{4} b_j, \tag{21}$$

where a_j, b_j are chosen so that the solitons sit symmetrically at the vertices of a square in the basic cell. A treatment parallel to that of the previous section leads to

$$\left.\begin{array}{l} a'_j{=}a'_1 \exp(i\varphi_j) \\ b'_j{=}b'_1 \exp(i\varphi_j) \end{array}\right\}; \quad \varphi_j{=}(j{-}1)\frac{\pi}{2},\ j{=}1,2,3,4. \tag{22}$$

The condition between the zeros and the poles is again verified $\forall\ a_1',\ b_1'$:

$$\sum_{j=1}^{4} a_j' = (0,0) = \sum_{j=1}^{4} b_j'.$$

Both the initial velocity and the time dependence are introduced by boosting:

$$\left.\begin{array}{rcl} a_j & \rightarrow & a_j + v_j t \\ b_j & \rightarrow & b_j + v_j t \end{array}\right\}; \quad v_j = -v_0 \exp(i\varphi_j), \tag{23}$$

where equation (16) should be kept in mind.

As pointed out in Sec. 2, four lumps involve a large energy, and while evolving in time they become too spiky before we can learn anything much about the scattering process. We have therefore studied this system in the Skyrme version of the theory, where the solitons are stable and may be examined for as long as required. Instead of the Lagrangian density (4) we have thus taken:

$$\mathcal{L} = \frac{|W_t|^2 - 2|W_z|^2 - 2|W_{\bar{z}}|^2}{(1+|W|^2)^2} - 8\theta_1 \frac{|W_z|^2 - |W_{\bar{z}}|^2}{(1+|W|^2)^4}(|W_t|^2 + |W_z|^2 - |W_{\bar{z}}|^2). \tag{24}$$

The configuration (6) is no longer an exact solution of the field equation derived from (24), albeit it is a very good approximation to it. Let us also stress that the presence of a small θ_1 term does not affect either the trajectory of the lumps before the collision or their scattering angle.

Taking

$$\left.\begin{array}{l} a_1 = (3.10, 3.10) \\ b_1 = (1.65, 1.575) \\ \theta_1 = 10^{-3} \\ v_0 = 0.35\exp(i\pi/4) \end{array}\right\}, \tag{25}$$

entails the state of identical 'baby skyrmions' illustrated in Fig. 4. The solitons W_2, W_3 and W_4 are rotated $90°, 180°$ and $270°$ with respect to W_1, which we have conveniently placed in the first quadrant, roughly on the central diagonal joining the grid points (0,0)-(4,4).

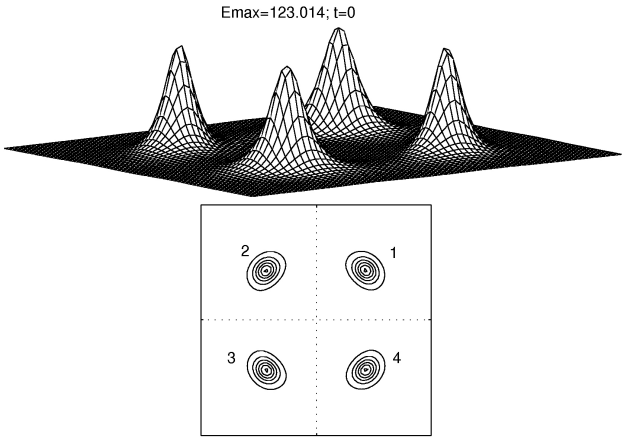

FIGURE 4. The energy distribution for N=4 at $t = 0$.

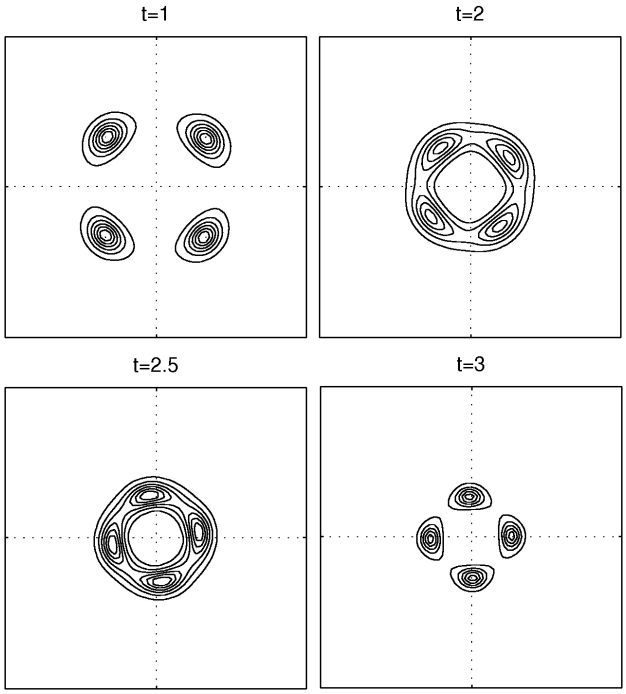

FIGURE 5. The evolution of the four lumps of Fig. 4 gets underway.

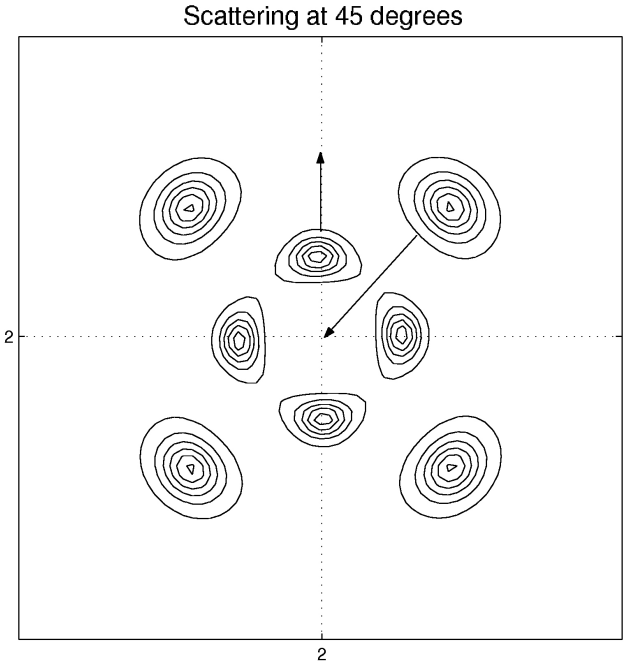

FIGURE 6. Scattering at $\pi/4$ radians.

The system (21) gets moving via (23), and zeroes in on the middle of the mesh, where the four skyrmions bump head-on into each other. This dynamics makes the solitons scatter off and emerge towards the vertices of the dual square, at $45°$ with respect to the initial direction of motion, as depicted in

diagram 5. Figure 6 superimposes both the initial state (t=0) and the final state ($t = 3$), allowing greater clarity in the appreciation of the scattering angle $\pi/4$.

Unlike the outcome of the previous section, the dual square scattering on T_2 is not so surprising. For although the initial data doesn't have D_4 symmetry, it does have 4-fold rotational symmetry and zero angular momentum. Note that the boundary conditions (5) break the $SO(2)$ rotational symmetry of the plane into a 4-fold rotational symmetry.

6. Geodesic approximation

Note that, in analogy to the S_2 case, when the speed v in (17) and (22) is set to zero, our initial configuration is a static solution of the equations of motion. If we change a_j, b_j to a new value given by (17) or (22) for a particular value of t the new configuration is again a static solution of the equations of motion. Hence as v changes, the changes (17) and (22) connect configurations which correspond to static solutions of the equations of motion. Thus it is reasonable to expect that a system set off with a small v will follow such a change. This expectation goes under the name of geodesic approximation (the system evolves by changing its zero-mode parameters). Its validity is not expected to depend too much on whether the model is defined on S_2 or T_2.

So far we have been concerned with solitons of equal size. Let us now look into the more general situation of energy lumps of different sizes, illustrating the proceedings by studying the case $N = 3$.

First we set up the initial configuration and evolve it through our standard numerical simulation. Then we choose a set of collective coordinates to reproduce the results of our simulations (trajectory, scattering), offering an explanation in the framework of the geodesic approximation.

6.1. Numerical simulation

Our 3-soliton system is still given by a function of the form (12), but with a layout not as symmetrical as before. Instead of (14) we put

$$\left.\begin{array}{rcl} a'_j &=& a'_1 \exp{(i\alpha_j)} \\ b'_j &=& b'_1 \exp{(i\alpha_j)} \end{array}\right\};$$

$$\alpha_j = (j-1)\frac{2\pi}{3} + (-1)^{(j-1)}(1-\delta_{1j})\xi, \qquad (26)$$

with j=1,2,3 and the numbers $a'_1,\ b'_1$ being fixed as customary. The initial three-soliton configuration can be written as

$$W = \frac{\sigma(z-a_1)}{\sigma(z-b)}\frac{\sigma(z-a_2)}{\sigma(z-b_2)}\frac{\sigma(z-a_3)}{\sigma(z-b_3)}$$

$$= \frac{\sigma(z'-a'_1)}{\sigma(z'-b')}\frac{\sigma(z'-a'_1e^{i\alpha_2})}{\sigma(z'-b'_1e^{i\alpha_2})}\frac{\sigma(z'-a'_1e^{-i\alpha_2})}{\sigma(z'-b'_1e^{-i\alpha_2})}, \qquad (27)$$

where

$$b' = a'_1 + 2(a'_1 - b'_1)\cos\alpha_2, \quad [\alpha_2 = \frac{2\pi}{3} - \xi], \qquad (28)$$

ensures that the zeros and poles comply with the constraint in Ref. 6). As usual we switch between primed and unprimed numbers through formula (16), plus b'=$b-c$ and z'=$z-c$. We have also used the fact that $\exp(i\alpha_3) = \exp(-i\alpha_2)$.

Note that equating ξ to zero simplifies α_j to

$$(j-1)2\pi/3 = \beta_j$$

of (14), whereupon the elliptic function (27) reduces to the field (12) simply because

$$\cos\alpha_2 = \cos\beta_2 = -1/2 \quad \rightarrow \quad b' = b'_1$$

according to (28).

An angle $\xi \neq 0$ generates solitons of different sizes which no longer enjoy the positional symmetry boasted by the arrangement (14). In the set-up (14), where ξ=0 and the solitons have the same size, the required relationship $\sum a'_j = \sum b'_j$ looks after itself as shown in (15). For $\xi \neq 0$, a demand of the kind (28) is needed.

Now we have evolved the solitons (27) in the pure version of the CP^1 model, with the solitons being sent into collision in the regular fashion:

$$\left.\begin{array}{rcl} a_j &\rightarrow& (a'_1 - v_0 t)\exp{(i\alpha_j)} + c \\ b &\rightarrow& (b' - v_0 t) + c \\ b_s &\rightarrow& (b'_1 - v_0 t)\exp{(i\alpha_s)} + c \end{array}\right\};$$

$$j = 1,2,3; \quad s = 2,3. \quad (29)$$

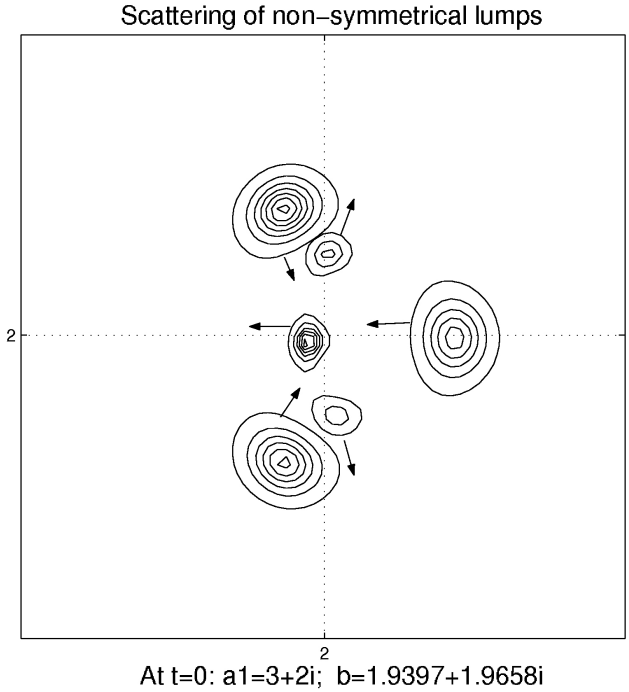

FIGURE 7. Numerical simulation for solitons rotated an angle $\xi = 10^\circ$ with respect to the symmetrical configuration of Fig. 1. They do not scatter at 60°.

The associated energy distribution is shown for a typical case by the contour plot of Fig. 7, which corresponds to a choice of parameters (20) in addition to $\xi = 10^\circ$.

The starting configuration is represented by the three wider structures whereas the final, scattered state is the narrower trio plotted therein. The sense of motion is clearly indicated by the arrows. We note that for both configurations the solitons are rotated an extra angle ξ with respect to W_1, as compared to their partners of Fig. 3. And, unlike the latter, it is not the case that the three initial lumps have the same size; nor they are situated at the vertices of an equilateral triangle. Apparent as well from our simulations is that the scattering angle differs from $\pi/3$. This is a consequence of considering nonsymmetrical solitons, whose collisions are not elastic and thus involve energy transfer.

Clearly the distance among the solitons differ from different pairs of them, and so their interactions are not the same resulting in a different scattering pattern. Can we explain this difference? In the next subsection, we show that an explanation can be provided in terms of, appropriately chosen, collective coordinates, with the motion following appropriate geodesics.

6.2. Collective coordinates

In order to make a wise selection of collective coordinates let us consider closely the positions and sizes of the solitons defined in the previous subsection.

The location of the solitons (27) is clearly

$$\frac{a_1' + b'}{2}, \quad \frac{a_1' + b_1'}{2} e^{i\alpha_2}, \quad \frac{a_1' + b_1'}{2} e^{-i\alpha_2}, \tag{30}$$

and their sizes are

$$\left| \frac{a_1' - b'}{2} \right|, \quad \left| \frac{a_1' - b_1'}{2} \right|, \quad \left| \frac{a_1' - b_1'}{2} \right|. \tag{31}$$

Put

$$a_1' = k - \chi, \qquad b_1' = k + \chi, \tag{32}$$

so the positions (30) adopt the form

$$k - \chi[1 + 2\cos(\alpha_2)], \qquad k e^{i\alpha_2}, \qquad k e^{-i\alpha_2}, \tag{33}$$

while the sizes (31) read

$$|2\chi \cos(\alpha_2)|\,, \qquad |\chi|\,, \qquad |\chi|\,. \tag{34}$$

Consistently, for $\xi = 0$ the description (33)-(34) corresponds to objects of the same size $|\chi|$, which are symmetrically situated at k and $k\exp(\pm i2\pi/3)$ (with respect to the centre). For simplicity, two out of the three lumps have the same size.

A possible collective coordinate description involves treating k, χ, and α_2 as collective coordinates. Thus, in the simulation we expect α_2 and χ to remain approximately constant, and k to vary. We are suggesting that the scattering can be understood as proceeding (on average) with only k depending on time and varying from (take k real for simplicity) $k > 0$ to $k < 0$. It is easy to show, although a bit tedious in practice (this involves estimating various elliptic integrals which can be done partially analytically, partially numerically), that both on $\Re_2$ and T_2 the kinetic energy of the motion just described is finite. So such behaviour is possible.

We have carried out our collective coordinates "motion" using the specific values

$$\chi = (0.55, 0), \quad k = (u, 0),\ u \in [1, -1], \tag{35}$$

where u varies across the interval in steps of 0.2. We see from (33) and (35) that the configurations for $u > 0$ ($u < 0$) correspond to incoming (outgoing/scattered) lumps. The value $u \approx 0$ represents the situation where the solitons have collided and are on top of each other, coalescing in the centre of the mesh. It is largely the behaviour of W at $u \approx 0$ what determines the scattering angle.

The states for k=(1,0) (incoming lumps) and k=(-0.2,0) ("scattered" lumps) are depicted in Fig. 8 for the case $\xi = 10^\circ$. As long as the path followed by the lumps and the scattering angle is concerned, the similarity with the numerically evolved situation of Fig. 7 is clear. Also, since we are mostly interested in the relative position of the solitons and their scattering angles, it is immaterial that the breadths of the solitons in Fig. 7 differ from the solitons of Fig. 8.

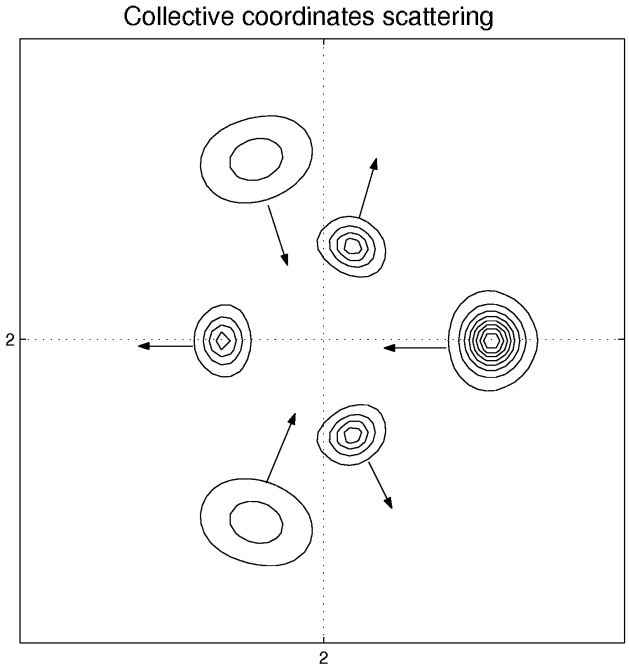

FIGURE 8. "Scattering" according to our collective coordinates view for $\xi = 10^\circ$, to be compared with the numerical result shown in Fig. 7. The incoming lumps are pictured for $k = (1, 0)$ and the outgoing structures correspond to $k = (-0.2, 0)$. It is not important that the widths of these lumps are not the same as their siblings of Fig. 7: we are interested in the relative positions and scattering angles.

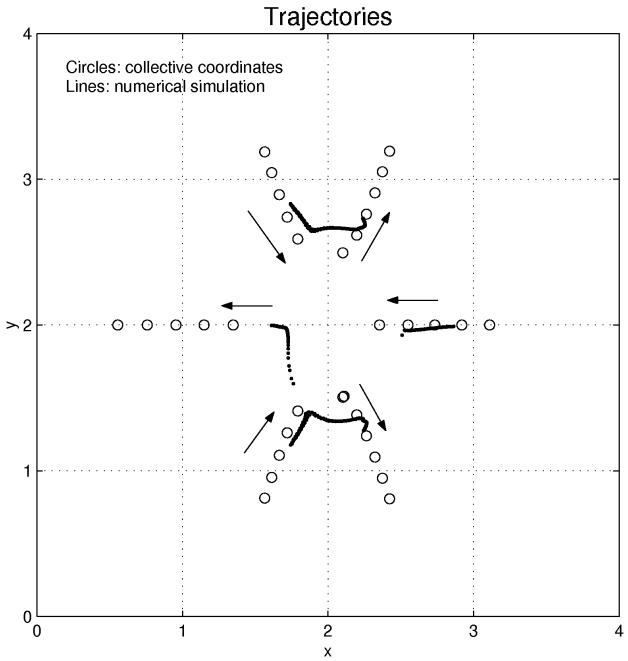

FIGURE 9. Trajectory plots ($\xi = 10^\circ$) sketching the path followed by the humps presented in Figs. 7 and 8. The itinerary according to our geodesic approximation (circles) shows very good agreement with the motion obtained via numerical simulation (solid lines).

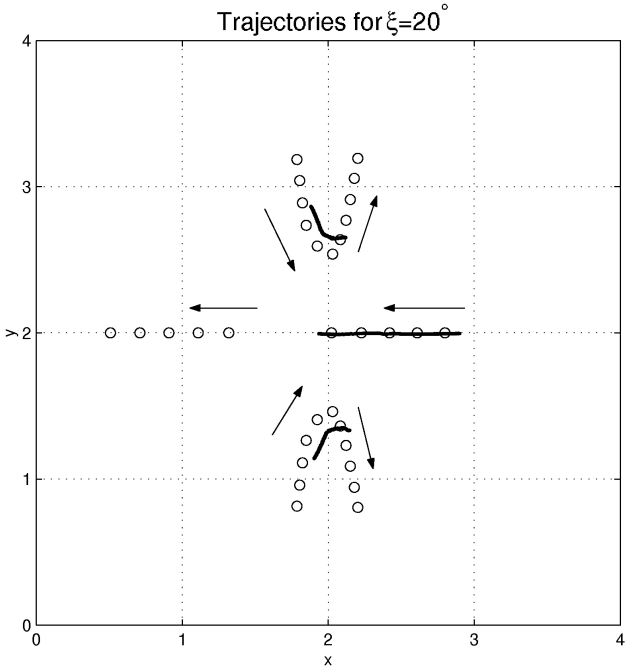

FIGURE 10. Plots comparing the trajectory obtained via numerical simulations (solid lines) and the trajectory gotten using the geodesic approximation (circles) for $\xi = 20^\circ$.

A more detailed comparison can be made via Fig. 9, which shows consecutive snapshots [corresponding to k=(1,0), (0.8,0), ..., (-0,2),(-0.4,0)...(-1,0)] of lump positions. The collective coordinate motion has been ticked with small circles and the motion according to the time evolution of subsection 6.1 has been sketched with solid lines. Note that after scattering the path of the numerically evolved lumps (continuous lines) cannot be followed much farther; this is because the solitons get very spiky and the simulation breaks down.

Our simulations have been carried out for several values of ξ and have been compared with the corresponding collective coordinate motion. We have always found the trajectories from both approaches to be in agreement, thus supporting our choice of collective coordinates. Another illustration is provided by Fig. 10 for the case $\xi = 20^\circ$.

7. Conclusions

In this article we have studied head-on collisions between solitons in the (2+1)-D CP^1 model with periodic boundary conditions, that is, with the model defined on a flat torus T_2.

Through numerical simulations we have found that solitons of equal sizes (at the initial time) scatter at an angle π/N (dual-polygon scattering), where N is the soliton number or topological charge of the system. In this paper we have focused on $N = 3, 4$ (the case $N = 2$ has been considered previously [4], and it has been found to comply with the $\pi/2$ scattering).

Unlike the usual model on $\Re_2$, our model with periodic boundary conditions breaks the $SO(2)$ rotational invariance of the plane, leaving us with a numerical mesh with directed sides where the initial soliton configuration has no symmetry under the dihedral group D_N. It is remarkable to still find π/N scattering on T_2, especially for $N = 3$; for $N = 4$, since the $SO(2)$ symmetry breaks into a four-fold rotational symmetry, the results are noteworthy but less unexpected. In any case, we need to study this matter further through numerical experiments with lumps situated near the borders of the cell, and check for deviations from D_N scattering.

We have also considered solitons of different sizes (at the initial time) and have observed that the scattering angle is no longer π/N, outcome arising from the fact that there is energy transfer in collisions between unsymmetrical solitons.

By reparametrising the quantities describing the positions of the solitons using a judicious set of collective coordinates, we have been able to reproduce the above numerical results, thus offering an explanation of the scattering process. We have illustrated this approach using a 3-soliton field.

These results raise important questions pertaining to the interplay between the symmetry of the initial configuration and the lack of symmetry of the torus itself. As pointed out at the end of Sec. 4, the non-isotropy of the torus might affect the evolution of the lumps if they are initially placed near the boundary of the mesh. What about systems with $N = 5, 6, \ldots$? Numerical experiments on a periodic, rectangular grid would also be worth performing. We hope to report on these matters in the near future.

Acknowledgements

Work for this paper was carried out during our visits to Durham and Maracaibo, and it was supported by the Royal Society of London, FONACIT and LUZ-CONDES. Many thanks.

∗ Permanent address: Departamento de Física, FEC, Universidad de Zulia, Maracaibo, Venezuela.

1. Y.M. Cho (editor), Proceedings of the 2nd Winter School on Mathematical Physics, Sorak Mountain Resort, Korea 22-26 Feb 1991, *Physics in (2+1) dimensions* (World Scientific 1992).
2. R.A. Leese, *et al. Nonlinearity* **3** (1990) 387.
3. T.H.R. Skyrme, *Nucl Phys* **31** (1962) 556.
4. R.J. Cova and W.J. Zakrzewski, *Nonlinearity* **10** (1997) 1305.
5. J.M. Speight, *Comm Math Phys* **194** (1998) 513.
6. R.J. Cova, *Eur Phys Jour B* **23** (2001) 201.
7. A. Kudryavtsev, B. Piette, and W. Zakrzewski, *Phys Lett A* **183** (1993) 119.
8. E. Goursat, *Functions of a complex variable* (Dover Publications, 1916).
9. D.F. Lawden, *Elliptic functions and applications* (Springer Verlag, 1989)
10. A. Erdélyi, *et al.*, *Higher transcendental functions*, vol II (Mc Graw Hill, 1953).
11. B. Piette and W. Zakrzewski, *Chaos, solitons and fractals* **5** (1995) 2495.